Progress In Electromagnetics Research, Vol. 132, 347–368, 2012

SPATIAL CORRELATION OF MULTIPLE ANTENNA ARRAYS IN WIRELESS COMMUNICATION SYSTEMS

J.-H. Lee[1, *] and C.-C. Cheng[2]

[1]Department of Electrical Engineering, Graduate Institute of Communication Engineering, and Graduate Institute of Biomedical Electronics and Bioinformatics, National Taiwan University, No. 1, Sec. 4, Roosevelt Road, Taipei 10617, Taiwan

[2]Graduate Institute of Communication Engineering, National Taiwan University, No. 1, Sec. 4, Roosevelt Road, Taipei 10617, Taiwan

Abstract—This paper investigates the spatial correlation characteristics of multiple antenna arrays deployed in wireless communication systems. First, we derive a general closed-form formula for the spatial correlation function (SCF) of a multiple antenna array with arbitrary array configuration under uniform signal angular energy distribution. Based on this formula, we then explore the characteristics of the SCF for several multiple antenna arrays with different array geometries. It is found that a multiple antenna array with a three-dimensional (3-D) array geometry can reduce the magnitude of its SCF and hence, improve the ergodic channel capacity (ECC) of wireless communication systems. Accordingly, we present a method to find the optimum 3-D antenna array geometry for maximizing the ECC of a wireless communication system. This method develops a novel objective function to incorporate with a particle swarm optimization (PSO) for solving the resulting optimization problem. Simulation results are provided for confirming the validity and the effectiveness of the proposed method.

1. INTRODUCTION

For the next generation of wireless communication technologies, a communication system employing multiple antenna arrays has been recognized as an appropriate manner to enhance the system's channel capacity and combat the multipath fading [1, 2]. Moreover, a wireless

Received 6 August 2012, Accepted 20 September 2012, Scheduled 2 October 2012

* Corresponding author: Ju-Hong Lee (juhong@cc.ee.ntu.edu.tw).

communication system using multiple antenna arrays at both the transmitter and receiver increases data rate and signal quality without requiring additional bandwidth [3]. However, the diversity reception method of [1, 2] suffers from the degradation of diversity gain due to the spatial correlation of the fading signals between the array elements with limited spacing. It has been shown that spatial correlation is a function of antenna spacing, array geometry, and the angular energy distribution and affects the performance of spatial antenna arrays [4–7].

Several reports [7–9] have presented the results regarding the characteristics of the spatial correlation function (SCF) of uniform linear arrays (ULAs). In [10], exact expressions of the spatial correlation coefficients were derived for different spatial distributions for ULAs. In contrast, due to that wireless base stations need azimuthally omni-directional antennas with sufficient power and sufficient beam width in the elevation plane so as to cover as wide an area as possible, there has been increased interest in using uniform circular arrays (UCAs). The spatial correlation characteristics of UCAs with a single ring have been reported by several research papers [7, 11–13]. However, by using a UCA to obtain a frequency invariant characteristic over a large bandwidth, the dynamic range of the compensation filters will be very large and it leads to considerable noise amplification. It was shown in [14–16] that this problem can be overcome if uniform concentric ring arrays (UCRAs) are used. The closed-form formulas expressing the spatial correlations of UCRAs in the uniform angle distribution and truncated Gaussian angle distribution have been presented in [17]. Although the results in the above papers are important for evaluating the channel capacity of wireless communication systems, they consider only the azimuth of arrival (AOA).

Recent research work shows that the performance of the handset antenna arrays for multiple-input-multiple-output (MIMO) systems is elevation dependent because the handset could be randomly oriented [18]. Moreover, the recent measurement results presented by [19] have shown that about 65% of the energy was incident with elevation angle larger than 10°. On the other hand, the results of [20] have shown that about 90% of the energy was incident with elevation angle between 0° and 40°. Several reports have considered the impact of both AOA and elevation of arrival (EOA) on the characteristics of the SCF for several antenna array configurations like the electromagnetic vector sensor (EVS), ULA, UCA, and uniform rectangular array (URA) [21–24, 37]. Nevertheless, a closed-form expression of SCF for multiple antenna arrays with arbitrary

three-dimensional (3-D) geometry is not available in the literature. Moreover, many researchers pay attention to finding the optimum antenna array geometry to reduce the spatial correlation and hence, maximize the channel capacity of wireless communication systems. Although maximizing the channel capacity for wireless communication systems with two-dimensional (2-D) antenna arrays was recently presented in [34], there are practically no papers concerning the optimum 3-D geometry of a multiple antenna array for maximizing the channel capacity of a wireless communication system. Therefore, there are no simulation results of using other techniques available in the literature for making comparison in the 3-D case.

In this paper, we derive a closed-form expression for the SCF of a 3-D antenna array under a uniform angular distribution for both AOA and EOA. Based on this formula, we then explore the characteristics of the SCF for several multiple antenna arrays with different array geometries. It is found that a multiple antenna array with 3-D array configurations can reduce the magnitude of its SCF and hence, improve the ergodic channel capacity (ECC) of wireless communication systems. A method is developed to find the optimum 3-D geometry of a multiple antenna array for maximizing the ECC of a wireless communication system. This method uses a novel fitness function to incorporate with a particle swarm optimization (PSO) for solving the resulting optimization problem. Simulation results are provided for confirming the validity and the effectiveness of the proposed method.

This paper is organized as follows. Section 2 derives the SCF of an antenna array with 3-D array configurations. A method is presented in Section 3 to find the optimum 3-D antenna array geometry for maximizing the ECC of a wireless communication channel. Section 4 shows several simulation examples for illustration and confirmation. We conclude the paper in Section 5.

2. SPATIAL CORRELATION FUNCTION

2.1. Antenna Array with 3-D Array Configurations

Let the mth array element of an antenna array be located at the position $(x_m,\ y_m,\ z_m)$ in the three dimensional (3-D) $(\mathbf{X},\ \mathbf{Y},\ \mathbf{Z})$ coordinate system and the associated position vector be denoted by $\mathbf{r}_m = [x_m\, y_m\, z_m]^T$, where the superscript "T" denotes the transpose operation. Figure 1 shows the 3-D $(\mathbf{X},\ \mathbf{Y},\ \mathbf{Z})$ coordinate system with four array elements for illustration. Accordingly, the difference vector between the position vectors of the nth and the mth array elements

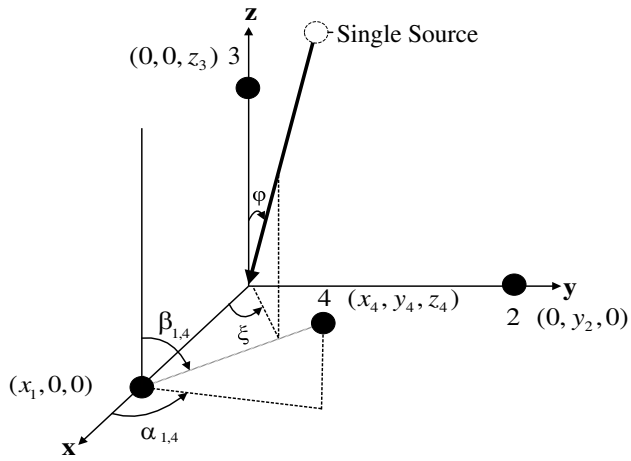

Figure 1. The 3-D (**X**, **Y**, **Z**) coordinate system with 4 array elements for illustration.

can be expressed by

$$\mathbf{d}_{m,n} = \begin{bmatrix} d_x \\ d_y \\ d_z \end{bmatrix} = \begin{bmatrix} x_n \\ y_n \\ z_n \end{bmatrix} - \begin{bmatrix} x_m \\ y_m \\ z_m \end{bmatrix} = \begin{bmatrix} r_{m,n}\sin(\beta_{m,n})\cos(\alpha_{m,n}) \\ r_{m,n}\sin(\beta_{m,n})\sin(\alpha_{m,n}) \\ r_{m,n}\cos(\beta_{m,n}) \end{bmatrix}, \quad (1)$$

where $r_{m,n}$ denotes the distance between the nth and the mth array elements. $\alpha_{m,n}$ represents the angle between $\mathbf{d}_{m,n}$ and the **X** axis, and $\beta_{m,n}$ represents the angle between $\mathbf{d}_{m,n}$ and the **Z** axis, respectively. Assume that the direction angles of a signal source are designated as the azimuth angle ξ and the elevation angle φ, respectively. Hence, the propagation vector of the signal source with the direction angle (φ, ξ) in the 3-D system of Figure 1 can be expressed by [35]

$$\mathbf{k}(\varphi,\xi) = -\frac{2\pi}{\lambda}\begin{bmatrix} \sin(\varphi)\cos(\xi) \\ \sin(\varphi)\sin(\xi) \\ \cos(\varphi) \end{bmatrix} \quad (2)$$

where λ denotes the signal wavelength. The minus sign arises because of the impinging direction of the signal source. Without loss of generality, we set the origin of the 3-D (**X**, **Y**, **Z**) coordinate system as the phase reference point. As a result, the phase delay of a signal source with the direction angle (φ, ξ) impinging on the mth array element can be expressed by [35]

$$\begin{aligned} v_m(\varphi,\xi) &= \exp\{-j(\mathbf{r}_m \cdot \mathbf{k}(\varphi,\xi))\} \\ &= \exp\{-j2\pi(x_m\sin(\varphi)\cos(\xi) + y_m\sin(\varphi)\sin(\xi) + z_m\cos(\varphi))/\lambda\}, \end{aligned} \quad (3)$$

where "$\cdot$" denotes the inner product of two vectors. $j = \sqrt{-1}$.

2.2. Derivations of Spatial Correlation Function

Based on the expression for the phase delay of the mth array element given by (3), the spatial correlation between the mth array element and the nth array element is given by [21]

$$\begin{aligned} R_s(m,n) &= E\{v_m(\varphi,\xi)v_n(\varphi,\xi)^*\} \\ &= \int_{\varphi}\int_{\xi} v_m(\varphi,\xi)v_n(\varphi,\xi)^* P(\varphi,\xi)\sin\varphi d\varphi d\xi, \end{aligned} \tag{4}$$

where $P(\varphi, \xi)$ denotes the probability density function (PDF) associated with the angular distribution of the incident signal. It has been shown that the spatial correlation and the statistics of signal angular distribution are closely related. Moreover, signal angular distribution depends on the environment of a wireless communication system with fading phenomenon. We concentrate on the uniform signal angular distribution in this paper. This model has been considered for deriving two-dimensional (2-D) spatial correlations [11]. It is also shown in [36] that the key parameter for the system performance is the standard deviation of the angle spread of the incident signal and not the type of PDF under investigation. For 3-D case, we assume that the PDF $P(\varphi, \xi)$ has the elevation angle φ uniformly distributed in $[\varphi_0 - \Delta\varphi, \varphi_0 + \Delta\varphi]$ and the azimuth angle ξ uniformly distributed in $[\xi_0 - \Delta\xi, \xi_0 + \Delta\xi]$, where $\Delta\varphi$ and φ_0 are the elevation spread (ES) and the mean of the elevation angular distribution, respectively, $\Delta\xi$ and ξ_0 are the azimuth spread (AS) and the mean of the azimuth angular distribution, respectively. We also assume that φ and ξ are independent of each other [22]. Thus, the probability density function (PDF) $P(\varphi, \xi)$ can be decomposed to $P(\varphi)P(\xi)$. Substituting (3) into (4) becomes

$$\begin{aligned} R_s(m,n) &= G\int_{\xi_0-\Delta\xi}^{\xi_0+\Delta\xi}\int_{\varphi_0-\Delta\varphi}^{\varphi_0+\Delta\varphi} \exp\left\{-j\frac{2\pi}{\lambda}(\mathbf{r}_m\cdot\mathbf{k}(\varphi,\xi))\right\} \\ &\times \exp\left\{j\frac{2\pi}{\lambda}(\mathbf{r}_n\cdot\mathbf{k}(\varphi,\xi))\right\}\sin(\varphi)d\varphi d\xi \\ &= G\int_{\varphi_0-\Delta\varphi}^{\varphi_0+\Delta\varphi}\int_{\xi_0-\Delta\xi}^{\xi_0+\Delta\xi} \exp\left\{j\frac{2\pi}{\lambda}r_{m,n}(\sin(\beta_{m,n})\cos(\alpha_{m,n})\sin(\varphi)\cos(\xi)\right. \\ &\left.+\sin(\beta_{m,n})\sin(\alpha_{m,n})\sin(\varphi)\sin(\xi)+\cos(\beta_{m,n})\cos(\varphi)\right\}\sin(\varphi)d\varphi d\xi \\ &= G\int_{\varphi_0-\Delta\varphi}^{\varphi_0+\Delta\varphi} \exp\left\{j\frac{2\pi}{\lambda}r_{m,n}\cos(\beta_{m,n})\cos(\varphi)\right\}\sin(\varphi) \end{aligned}$$

$$\times \int_{\xi_0-\Delta\xi}^{\xi_0+\Delta\xi} \exp\left\{ j\frac{2\pi}{\lambda} r_{m,n} \sin(\beta_{m,n}) \sin(\varphi) \cos(\xi - \alpha_{m,n}) \right\} d\varphi d\xi, \quad (5)$$

where $G = 1/(4\Delta\xi \sin(\varphi) \sin(\Delta\varphi))$ due to independent and uniform angular distribution [22]. Let $\tilde{\xi} = \xi - \alpha_{m,n}$. (5) can be rewritten as

$$R_s(m,n) = G \int_{\varphi_0-\Delta\varphi}^{\varphi_0+\Delta\varphi} \exp\left\{ j\frac{2\pi}{\lambda} r_{m,n} \cos(\beta_{m,n}) \cos(\varphi) \right\} \sin(\varphi) \int_{\xi_0-\Delta\xi-\alpha_{m,n}}^{\xi_0+\Delta\xi-\alpha_{m,n}} \exp\left\{ j\frac{2\pi}{\lambda} r_{m,n} \sin(\beta_{m,n}) \sin(\varphi) \cos\left(\tilde{\xi}\right) \right\} d\varphi d\tilde{\xi}. \quad (6)$$

Following the Jacobi-Anger expansion, we have

$$e^{jz\cos(x)} = \sum_{k=-\infty}^{\infty} j^k J_k(z) e^{jkx} \quad (7)$$

Substituting (7) into the second integration of (6) yields

$$\begin{aligned} &\int_{\xi_0-\Delta\xi-\alpha_{m,n}}^{\xi_0+\Delta\xi-\alpha_{m,n}} \exp\left\{ j\frac{2\pi}{\lambda} r_{m,n} \sin(\beta_{m,n}) \sin(\varphi) \cos\left(\tilde{\xi}\right) \right\} d\tilde{\xi} \\ &= \sum_{k=-\infty}^{\infty} j^k J_k\left(\frac{2\pi}{\lambda} r_{m,n} \sin(\beta_{m,n}) \sin(\varphi)\right) \frac{2}{k} \sin(k\Delta\xi) \times \exp\{k(\xi_0 - \alpha_{m,n})\} \\ &= 2\Delta\xi J_0\left(\frac{2\pi}{\lambda} r_{m,n} \sin(\beta_{m,n}) \sin(\varphi)\right) \\ &+ 4\sum_{k=1}^{\infty} \left\{ j^k J_k\left(\frac{2\pi}{\lambda} r_{m,n} \sin(\beta_{m,n}) \sin(\varphi)\right) \frac{\sin(k\Delta\xi)}{k} \times \cos(k(\xi_0 - \alpha_{m,n})) \right\} \quad (8) \end{aligned}$$

Substituting (8) into (6) provides

$$\begin{aligned} R_s(m,n) = G \int_{\varphi_0-\Delta\varphi}^{\varphi_0+\Delta\varphi} &\exp\left\{ j\frac{2\pi}{\lambda} r_{m,n} \cos(\beta_{m,n}) \cos(\varphi) \right\} \sin(\varphi) \\ \times \Bigg[&2\Delta\xi J_0\left(\frac{2\pi}{\lambda} r_{m,n} \sin(\beta_{m,n}) \sin(\varphi)\right) \\ &+ 4\sum_{k=1}^{\infty} \left\{ j^k J_k\left(\frac{2\pi}{\lambda} r_{m,n} \sin(\beta_{m,n}) \sin(\varphi)\right) \frac{\sin(k\Delta\xi)}{k} \times \cos(k(\xi_0 - \alpha_{m,n})) \right\} \Bigg] d\varphi \end{aligned}$$

$$= \frac{\int_{\varphi_0-\Delta\varphi}^{\varphi_0+\Delta\varphi} \left[\begin{array}{l} \exp\left\{ j\dfrac{2\pi}{\lambda} r_{m,n}\cos(\beta_{m,n})\cos(\varphi) \right\}\sin(\varphi) \\ \times J_0\left(\dfrac{2\pi}{\lambda} r_{m,n}\sin(\beta_{m,n})\sin(\varphi) \right) \end{array} \right] d\varphi}{2\sin(\varphi_0)\sin(\Delta\varphi)}$$

$$+ \sum_{k=1}^{\infty} \left[\frac{\int_{\varphi_0-\Delta\varphi}^{\varphi_0+\Delta\varphi} \left\{ \begin{array}{l} \exp\left\{ j\dfrac{2\pi}{\lambda} r_{m,n}\cos(\beta_{m,n})\cos(\varphi) \right\}\sin(\varphi) \\ \times J_k\left(\dfrac{2\pi}{\lambda} r_{m,n}\sin(\beta_{m,n})\sin(\varphi) \right) \end{array} \right\} d\varphi}{\sin(\varphi_0)\sin(\Delta\varphi)} \times \right.$$
$$\left. \frac{}{j^k \cos(k(\xi_0 - \alpha_{m,n}))\sin \mathrm{c}(k\Delta\xi)} \right], \quad (9)$$

where $\mathrm{sinc}(x)$ denotes the sinc function defined by $\mathrm{sinc}(x) = \sin(x)/x$. To obtain a closed-form solution, we present an approximation for computing the integrations of (9). Consider the well-known Trapezoidal rule for approximation as follows:

$$\int_a^b f(x)dx \approx \frac{b-a}{N}\left[0.5f(x_0)+f(x_1)+\ldots+f(x_{N-1})+0.5f(x_N)\right]. \quad (10)$$

Based on (10), we let

$$\begin{cases} f(x) = e^{j\frac{2\pi}{\lambda} r_{m,n}\cos(\beta_{m,n})\cos(x)}\sin(x) J_0\left(\dfrac{2\pi}{\lambda} r_{m,n}\sin(\beta_{m,n})\sin(x)\right) \\ g_k(x) = e^{j\frac{2\pi}{\lambda} r_{m,n}\cos(\beta_{m,n})\cos(x)}\sin(x) J_k\left(\dfrac{2\pi}{\lambda} r_{m,n}\sin(\beta_{m,n})\sin(x)\right) \end{cases}. \quad (11)$$

Substituting (10) and (11) into (9) yields the following closed-form approximation of the spatial correlation function (SCF) for an antenna array with 3-D array configurations

$$R_s(m,n) \approx \frac{\left[0.5f(x_0) + f(x_1) + \ldots + f(x_{N-1}) + 0.5f(x_N)\right]}{N\sin(\varphi_0)\sin c(\Delta\varphi)}$$
$$+ \frac{\sum_{k=1}^{\infty} \left\{ \begin{array}{l} j^k \cos(k(\xi_0 - \alpha_{m,n}))\mathrm{sinc}(k\Delta\xi) \\ \left[0.5g_k(x_0) + g_k(x_1) + \ldots + g_k(x_{N-1}) + 0.5g_k(x_N)\right] \end{array} \right\}}{N\sin(\varphi_0)\mathrm{sinc}(\Delta\varphi)}. \quad (12)$$

For the case of a 2-D antenna array deployed in the 2-D ($\mathbf{X}$, $\mathbf{Y}$) coordinate system, we set the angle $\beta_{m,n}$ between $\mathbf{d}_{m,n}$ and the $\mathbf{Z}$ axis to $\beta_{m,n} = \pi/2$. Substituting $\beta_{m,n} = \pi/2$ into (11) gives

$$\begin{cases} f(x) = \sin(x) J_0\left(\dfrac{2\pi}{\lambda} r_{m,n}\sin(x)\right) \\ g_k(x) = \sin(x) J_k\left(\dfrac{2\pi}{\lambda} r_{m,n}\sin(x)\right) \end{cases}. \quad (13)$$

Consequently, a closed-form approximation of the SCF for 2-D antenna systems can be obtained by substituting (13) into (12). From the simulation results based on (12), we are able to observe that the SCF of using a 3-D array configuration has a smaller magnitude than that of using a 2-D array configuration under the same signal characteristics.

3. PROPOSED METHOD FOR ECC MAXIMIZATION

3.1. Channel Model of Wireless Communications

Assume that a wireless communication system has a multiple antenna array with N_t array elements at the transmitter and a multiple antenna array with N_r array elements at the receiver. The signal vector received at the receiver is given by

$$\mathbf{y} = \mathbf{H}\mathbf{s} + \mathbf{n}, \tag{14}$$

where $\mathbf{s}$ denotes the transmitted signal vector and $\mathbf{n}$ the received additive white Gaussian noise (AWGN) vector. The entries of $\mathbf{n}$ are independent identically distributed (iid) Gaussian random variables with zero mean and variance equal to one. $\mathbf{H}$ denotes the $N_r \times N_t$ coefficient matrix of a Rayleigh fading channel. Under the analytical Kronecker channel model which assumes separability in correlation induced by the transmitter and the receiver arrays, we can express $\mathbf{H}$ as follows [25, 26]:

$$\mathbf{H} = (\mathbf{R}_{rx})^{1/2}\mathbf{H}_w \left\{(\mathbf{R}_{tx})^{1/2}\right\}^H, \tag{15}$$

where the superscript "$\mathbf{H}$" denotes the complex conjugate transpose and $(\mathbf{A})^{1/2}$ the square root of matrix $\mathbf{A}$. $\mathbf{H}_w$ is a stochastic $N_r \times N_t$ matrix with iid complex Gaussian entries with zero mean and unit variance. The $N_r \times N_r$ and $N_t \times N_t$ matrices $\mathbf{R}_{rx}$ and $\mathbf{R}_{tx}$ are the spatial correlations of the multiple antenna arrays at the receiver and the transmitter sides, respectively. The corresponding full channel correlation matrix $\mathbf{R}$ is derived as

$$\mathbf{R} = \mathbf{R}_{tx} \otimes \mathbf{R}_{rx}, \tag{16}$$

where $\otimes$ denotes the Kronecker product. This Kronecker channel model of (15) not only simplifies analytical treatment or simulation of multiple-input-multiple-output (MIMO) wireless communication systems, but also allows for independent array optimization at the transmitter and the receiver.

3.2. Ergodic Channel Capacity

For simplicity, we consider the capacity of single-user MIMO channels. The single-user results are still of much interest for the insight they provide. Under the assumption of perfect state information at the receiver and no channel state information at transmitter, we have the MIMO ergodic channel capacity (ECC) for each realization computed by [27]

$$C = \log_2 \left\{ \det \left(\mathbf{I} + \rho \mathbf{H}^H \mathbf{H} \right) \right\}, \tag{17}$$

where the transmit power is divided equally among all the transmit antennas. Hence, ρ is set to $\rho = \frac{P}{N_t \sigma_n^2}$, where P denotes the total power transmitted at the transmitter and σ_n^2 the noise variance.

3.3. ECC Maximization Using Particle Swarm Optimization (PSO)

Here, we present a method to find the optimum configuration of a multiple antenna array at the receiver for maximizing the ECC shown by (17). Consider that the multiple antenna array at the transmitter is a UCA with radius R equal to $\lambda/2$, where λ is the signal wavelength. The angle spreads (AS) and $\Delta\xi$ and $\Delta\varphi$ of the azimuth and elevation angular distributions are set to 180° and 90°, respectively For simplicity, we let $N_r = N_t = N$. The $N \times N$ spatial correlation matrix $\mathbf{R}_{tx} = [R_{tx}(m, n)]$ for the UCA at the transmitter has its entry $R_{tx}(m, n)$ calculated by (12) with $f(x)$ and $g_k(x)$ given by (13) for $m, n = 1, 2, \ldots, N$. As to the $N \times N$ spatial correlation matrix $\mathbf{R}_{rx} = [R_{rx}(m, n)]$ for the multiple antenna array at the receiver has its entry $R_{rx}(m, n)$ calculated by (12) for m, $n = 1, 2, \ldots, N$. The optimum position of the mth array element is to be searched to maximize the ECC of (17). The space for searching the optimum position (x_{mo}, y_{mo}, z_{mo}) of the mth array element is set to a sphere with radius equal to $D_{\max}$, where the second subscript "o" in (x_{mo}, y_{mo}, z_{mo}) denotes the optimum position. The resulting optimization problem is highly nonlinear. We utilize the well-known particle swarm optimization (PSO) algorithm to deal with the highly nonlinear optimization problem.

3.4. Particle Swarm Optimization (PSO)

The basic idea of a PSO algorithm introduced by [28] is to utilize a swarm with multiple particles. It has become an efficient algorithm in solving difficult multidimensional optimization problems [32]. Using the information of social interaction between independent agents

(called particles) and the concept of an objective function or fitness, a PSO algorithm searches the optimum solution. It estimates each particle at each moment t ($t = 0, 1, 2, \ldots$) by using the value of the objective function at the ith particle's current position $\mathbf{x}_i(t) \in D$, where D denotes the search space. The velocity $\mathbf{v}_i(t)$ of the ith particle at the moment t depends on the velocity at the moment $(t-1)$, the position $\mathbf{x}_i(t)$, the best position $\mathbf{p}_i(t)$ found up to now, and the best position $\mathbf{g}(t)$ found up to now by the swarm. The update formula for $\mathbf{v}_i(t)$ is given by [29]

$$\mathbf{v}_i(t) = c_1\mathbf{v}_i(t-1) + c_2\{\mathbf{p}_i(t) - \mathbf{x}_i(t)\} + c_3\{\mathbf{g}(t) - \mathbf{x}_i(t)\}, \tag{18}$$

where $c_1 \in [0, 1]$ denotes the inertial weight, c_2 and c_3 are selected randomly at the moment by

$$c_k = d_k U(0, 1); \quad k = 2, 3, \tag{19}$$

where $U(0, 1)$ represents a random variable uniformly distributed in $[0, 1]$. d_2 and d_3 specify the relative weights between the personal best position and the global best position, respectively Accordingly, the position of the particle at the moment $(t+1)$ is defined by

$$\mathbf{x}_i(t+1) = \mathbf{x}_i(t) + \mathbf{v}_i(t) \tag{20}$$

We summarize the PSO algorithm step-by-step as follows [29]:

Step 1: Select the size of the swarm n (the number of particles), a threshold E and a time limit T to stop the algorithm when the estimation of any particle e_i becomes $e_i \geqq E$ or the time t becomes $t \geqq T$; let $t = 0$; randomly locate n particles in the search space and set an initial velocity to each particle according to the size of the search space.

Step 2: Get the estimation e_i ($i = 1, 2, \ldots, n$) for each particle by the objective function, and update $\mathbf{p}_i$ and $\mathbf{g}$.

Step 3: Stop the algorithm and take the output $\mathbf{g}$ as its solution if one of the following "stop conditions" is satisfied. Otherwise, go to the next step.

(a) the best estimation $e_{best} \geqq E$,

(b) $t \geqq T$.

Step 4: Let $t = t + 1$ and update $\mathbf{v}_i$ and $\mathbf{x}_i$ by (18) and (20), respectively.

Step 5: Go to *Step* 2.

3.5. The Objective Function

For the considered problem, the objective function of a PSO is set to an evaluation of the ECC in terms of the optimization parameters. In

the literature, a closed-form formula of the expectation of the ECC with $N_r = N_t = N$ is derived as [33], Eq. (21)

$$E[C] = \text{trace}\left\{\mathbf{\Lambda}^{-1}(\boldsymbol{\nu})\mathbf{\Lambda}^{(1)}(\boldsymbol{\nu})\right\}_{\nu=0} - N + 1, \tag{21}$$

where $\mathbf{\Lambda}(\nu)$ and $\mathbf{\Lambda}^{(1)}(\nu)$ are $N \times N$ matrices with the (i, j)th entries given by [33, Table 1]

$$\{\mathbf{\Lambda}(\nu)\}_{i,j} = \lambda_{tx,j}^{-1} \int_0^\infty (1 + \rho\lambda_{rx,i}z)^{\nu+N-1} \exp\{-z/\lambda_{tx,j}\}dz, \tag{22}$$

and

$$\begin{aligned} &\left\{\mathbf{\Lambda}^{(n)}(\nu)\right\}_{i,j} \\ &= \lambda_{tx,j}^{-1} \int_0^\infty (1+\rho\lambda_{rx,i}z)^{\nu+N-1} \ln^n(1+\rho\lambda_{rx,i}z) \exp\{-z/\lambda_{tx,j}\}dz, \end{aligned} \tag{23}$$

respectively, where $\rho = \frac{P}{N\sigma_n^2}$, P is the total power transmitted at the transmitter, and σ_n^2 noise variance. $\lambda_{tx,i}$ and $\lambda_{rx,i}$ are the ith eigenvalues of the spatial correlation matrix at transmitter end and receiver end, respectively, $i = 1, 2, \ldots, N$. $\mathbf{\Lambda}^{(n)}(\nu)$ represents the nth derivative of the square matrix $\mathbf{\Lambda}(\nu)$ with respect to ν. Another closed-form formula of the expectation of the ECC is derived as [30, Eq. (25)]

$$E[C] = \left\{\sum_{k=1}^{N} \det(\mathbf{\Psi}(k))\right\} \times \left\{\ln(2)\det(\mathbf{V})\prod_{i=1}^{N}\Gamma(N-i+1)\right\}^{-1}, \tag{24}$$

where $\det(\mathbf{X})$ denotes the determinant of the matrix $\mathbf{X}$. $\mathbf{\Psi}(k)$, $k = 1, 2, \ldots, N$, are $N \times N$ matrices with the (i, j)th entries given by [30, Eq. (26)]

$$\{\mathbf{\Psi}(k)\}_{i,j} = \begin{cases} \displaystyle\int_0^\infty \ln(1+\rho y)y^{N-1}e^{-y/\lambda_j}dy, & \text{if } i = k \\ \lambda_j^{N-i+1}\Gamma(N-i+1), & \text{if } i \neq k \end{cases}, \tag{25}$$

$\rho = \frac{P}{N\sigma_n^2}$, P is the total power transmitted at the transmitter, and σ_n^2 is noise variance. $\Gamma(\cdot)$ is the gamma function. $\mathbf{V}$ is an $N \times N$ matrix with determinant given by [30, Eq. (15)]

$$\det(\mathbf{V}) = \left(\prod_{i=1}^{N}\lambda_i^N\right)\prod_{1\le l<k\le N}\left(\frac{1}{\lambda_k} - \frac{1}{\lambda_l}\right) \tag{26}$$

where λ_i is the ith eigenvalue of the related spatial correlation matrix. ρ is the transmitting SNR per branch. It is obvious that we face a

very complicated computational process to calculate (21) or (24) if any of them is adopted as the objective function for the considered optimization problem. Therefore, we resort to another objective function with a reasonable computational complexity. According to the results derived by [31], we have the following closed-form upper bound for the expectation of the ECC

$$E[C] < \log\left(\sum_{k=0}^{N} k!\rho^k E_{tx,k} E_{rx,k}\right), \tag{27}$$

where $E_{tx,k}$ and $E_{rx,k}$ are given as follows [31]:

$$E_{tx,k} = \sum_{\boldsymbol{\alpha}_k} \lambda_{tx,\alpha_1}\lambda_{tx,\alpha_2}\ldots\lambda_{tx,\alpha_k} \text{ and } E_{rx,k} = \sum_{\boldsymbol{\alpha}_k} \lambda_{rx,\alpha_1}\lambda_{rx,\alpha_2}\ldots\lambda_{rx,\alpha_k}, \tag{28}$$

respectively, where $\boldsymbol{\alpha}_k = \{\alpha_1, \alpha_2, \ldots, \alpha_k\}$ is any possible set of numbers $\alpha_k \in \{1, 2, \ldots, N\}$, $k = 1, 2, \ldots N$. λ_{tx,α_k} and λ_{rx,α_k} represent the α_kth eigenvalues of the spatial correlation matrices $\mathbf{R}_{tx}$ and $\mathbf{R}_{rx}$, respectively. (28) reveals that computing the upper bound requires much less computational complexity as compared to those required by computing (21) and (24). Hence, we adopt the upper bound as the objective function of the PSO for performing the optimization process, i.e., we define

$$\text{Objective Function} = f(\mathbf{P}) = \log\left(\sum_{k=0}^{N} k!\rho^k E_{tx,k} E_{rx,k}\right), \tag{29}$$

where $\mathbf{P} = [x_1, y_1, z_1, x_2, y_2, z_2, \ldots, x_N, y_N, z_N]^T$ represents the $3N \times 1$ vector containing the positions of the N array elements. In the literature, there are practically no papers concerning the similar upper bound for maximizing the ECC of a wireless communication system using 3-D antenna arrays. The search space for the position (x_m, y_m, z_m) of the mth array element is inside a 3-D sphere with radius given by $D_{\max}$, i.e., we have to find the optimum position (x_{mo}, y_{mo}, z_{mo}) of the mth array element, $m = 1, 2, \ldots, N$, with the following constraint

$$\sqrt{x_{mo}^2 + y_{mo}^2 + z_{mo}^2} \leq D_{\max}. \tag{30}$$

3.6. The Optimization Process

Here, we present an optimization process based on the PSO algorithm described in Section 3.4 and the objective function proposed in Section 3.5. The optimization process finds the optimum positions in the 3-D space for the N array elements of the multiple antenna array at the receiver to maximize the objective function $f(\mathbf{P})$ given by (29). It is summarized step-by-step as follows:

Step 1: Set the following parameters: the number of array elements N, the mean of azimuth angle ξ_0, the mean of elevation angle φ_0, AS $\Delta\xi$ and ES $\Delta\varphi$, $D_{\max}$, the objective function $f(\mathbf{P})$ of (29), the number of particles $n = 16$, the time limit $T = 500$, the velocity limit $V_{\max} = D_{\max}/5$, the relative weights $d_2 = d_3 = 2$, and the inertial weight $c_1 \in [0, 1]$ is set according to the following formula:

$$c_1(t) = c_{1\text{start}} - \frac{c_{1\text{start}} - c_{1\text{end}}}{T} \times t, \tag{31}$$

where $c_1(t)$ represents the value of c_1 at the moment t. $c_{1\text{start}} = 0.9$ and $c_{1\text{end}} = 0.4$ denote two preset values related to c_1. The proposed time-varying inertial weight (31) leads to that the optimization process finds a satisfactory solution within a reasonable convergence speed according to our experience.

Step 2: Initialize the following parameters: The initial position $\mathbf{x}_1(1)$ of the 1st particle is set to a UCA on the azimuth plane and the initial position $\mathbf{x}_i$ (1) of the ith particle is randomly set in the search space, $i = 2, 3, \ldots, 16$. All the initial velocities $\mathbf{v}_i(t)$, $i = 1, 2, 3, \ldots, 16$, are set to zero. The initial best personal value f_i of the objective function $f(\mathbf{P})$ of (29) for the ith particle is set to 0, $i = 1, 2, 3, \ldots, 16$. The initial best global value f_g of the objective function $f(\mathbf{P})$ for swarm is set to 0. Set the initial time instant $t = 1$.

Step 3: Compute the value f_i of the objective function $f(\mathbf{P})$ at the position $\mathbf{x}_i(t)$, $i = 1, 2, 3, \ldots, 16$, at the time instant t according to the formula of (12) for computing the spatial correlation matrices $\mathbf{R}_{tx}$ and $\mathbf{R}_{rx}$ derived in Section 2.

Step 4: Compare $f(\mathbf{P})$ with f_i. Set f_i to the current $f(\mathbf{P})$ and the best personal position $\mathbf{p}_i(t)$ to the current position $\mathbf{x}_i(t)$ if $f(\mathbf{P}) > f_i$.

Step 5: Compare f_i, $i = 1, 2, \ldots, 16$, with f_g at the time t. Set f_g to f_i and the $\mathbf{g}(t)$ to $\mathbf{p}_i(t)$ if $f_i > f_g$.

Step 6: Update the velocity $\mathbf{v}_i(t)$ according to (18) and the position $\mathbf{x}_i(t)$ according to (20).

Step 7: Set $t = t+1$. Go to *Step 3* if $t < T$. Otherwise, terminate the optimization process.

During the optimization process, we set the number of particles $n = 16$ and the time limit T= 500. It is our experience that setting $n = 16$ and $T = 500$ provides satisfactory simulation results within a reasonable computation time. Moreover, our experience shows that setting $n > 16$ and $T > 500$ requires much more computation time and cannot produce a significant improvement over that with $n = 16$ and $T = 500$.

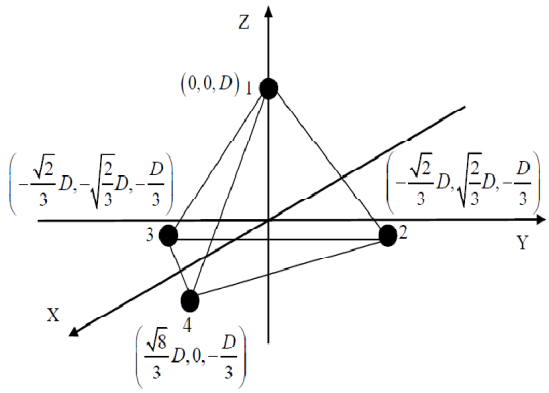

Figure 2. The multiple antenna array system with 4 elements for simulation.

4. SIMULATION RESULTS

Here, we present several simulation examples for illustration and confirmation.

Example 1: The multiple antenna array system with 4 array elements is shown in Figure 2 for illustration. We use (11) and (12) with $N = 2000$ to compute the spatial correlations under a uniform angular distribution. The positions for the 4 array elements are as follows:

Element 1 Position: $(0, 0, D)$, Element 2 Position: $(-\sqrt{2}D/3, \sqrt{2/3}D, -D/3)$, Element 3 Position: $(-\sqrt{2}D/3, -\sqrt{2/3}D, -D/3)$, Element 4 Position: $(\sqrt{8}D/3, 0, -D/3)$, where D in λ denotes the radius of the sphere with its surface containing the 4 array elements and λ the signal wavelength. Figures 3–8 depict the absolute values of the spatial correlation functions $R_s(1, 2)$, $R_s(1, 3)$, $R_s(1, 4)$, $R_s(2, 3)$, $R_s(2, 4)$, and $R_s(3, 4)$ versus the radius of the sphere for different combinations of AS and ES, respectively, where MEOA and MAOA represent the means of the elevation and azimuth angular distributions of the arrival, respectively. From these figures, we observe that the spatial correlation curves for the uniform angular distribution with larger angular spread show a common behavior that the spatial correlation decreases more rapidly as D increases. Moreover, each of the spatial correlations $|R_s(1, 4)|$, $|R_s(2, 3)|$, $|R_s(2, 4)|$, and $|R_s(3, 4)|$ decreases like a sinc vibration as the angular spread increases. Hence, the output signals of the array elements are heavily correlated if the angular spread is very small. In this case, the diversity gain of the

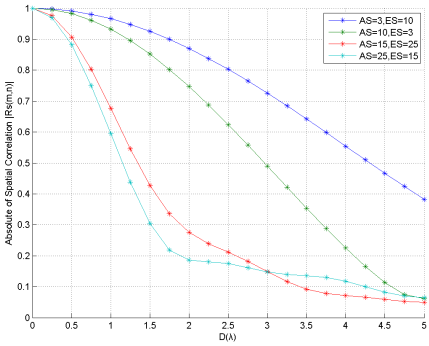

Figure 3. Spatial correlation between elements 1 and 2 with MEOA = 45° and MAOA = 0°.

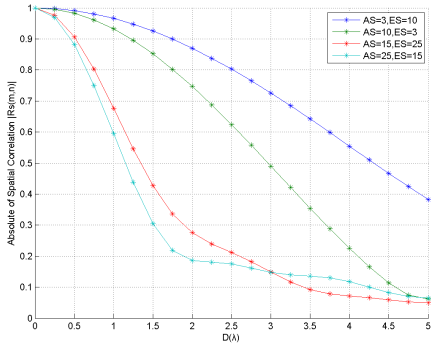

Figure 4. Spatial correlation between elements 1 and 3 with MEOA = 45° and MAOA = 0°.

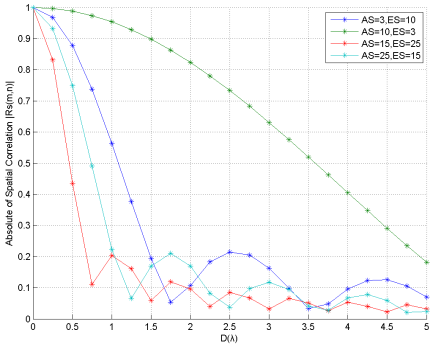

Figure 5. Spatial correlation between elements 1 and 4 with MEOA = 45° and MAOA = 0°.

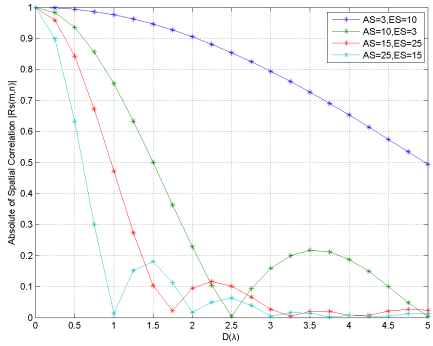

Figure 6. Spatial correlation between elements 2 and 3 with MEOA = 45° and MAOA = 0°.

3-D antenna array system suffers from degradation. In contrast, if the angular spread is rather large, the output signals of different array elements are weakly correlated. This leads to that a better diversity gain can be obtained.

Example 2: This example shows the results of using the proposed method presented in Section 3 for ECC maximization under a fixed $D_{\max}$. The parameters used are as follows: $N_{tx} = N_{rx} = 6$, MAOA = 90°, AS = 3°, ES = 5°, $D_{\max} = 5\lambda$, where λ denotes the signal wavelength. The signal-to-noise ratio (SNR) $\frac{P}{\sigma_n^2}$ is 10 dB. The number of Monte Caro runs for obtaining the sample average of the expectation of the ECC is set to 3000. Figure 9 depicts the ECC versus the MEOA. For comparison, the results of using ULA with

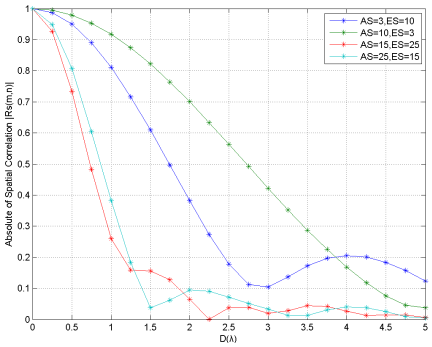

Figure 7. Spatial correlation between elements 2 and 4 with MEOA = 45° and MAOA = 0°.

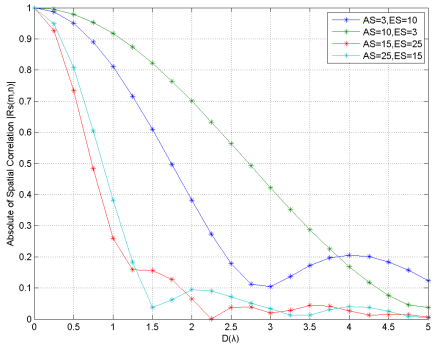

Figure 8. Spatial correlation between elements 3 and 4 with MEOA = 45° and MAOA = 0°.

length $2D_{\max} = 10\lambda$ and UCA with radius $D_{\max} = 5\lambda$ are included. We also present the results of using a multiple antenna array restricted to a 2-D area on the azimuth plane, i.e., $\sqrt{x_{mo}^2 + y_{mo}^2} \leq D_{\max}$ with radius $D_{\max} = 5\lambda$ on the azimuth plane and array element positions optimized by the process presented in Section 3.6. We observe that the proposed method provides the best ECC performance for a multiple antenna array with a 3-D geometry. Although the ECC with a 2-D multiple antenna array can be improved by using the proposed method, the resulting ECC is very close to that with a UCA. Table 1 lists the array element positions after performing the optimization process for this example with MEOA = 20°. We observe from this table that the obtained optimum 3-D array geometry is almost equal to a sphere with radius equal to $D_{\max} = 5\lambda$. In contrast, for the 2-D case, we note that the resulting optimum 2-D array geometry is almost the same as a 2-D UCA with radius equal to $D_{\max} = 5\lambda$ This confirms the results shown by Figure 9 for the 2-D case.

Example 3: This example shows the results of using the proposed method presented in Section 3 for ECC maximization under different $D_{\max}$. The parameters used are as follows: $N_{tx} = N_{rx} = 6$, MAOA = 90°, AS = 3°, ES = 5°, MEOA = 90°. The signal-to-noise ratio (SNR) $\frac{P}{\sigma_n^2}$ is 10 dB. The number of Monte Caro runs for obtaining the sample average of the expectation of the ECC is set to 3000. Figure 10 depicts the ECC versus the $D_{\max}$. For comparison, the results of using ULA with length $2D_{\max}$ and UCA with radius $D_{\max}$ are included. We also present the results of using a multiple antenna array restricted to a circular area, i.e., $\sqrt{x_{mo}^2 + y_{mo}^2} \leq D_{\max}$ on the azimuth plane and array element positions optimized by the

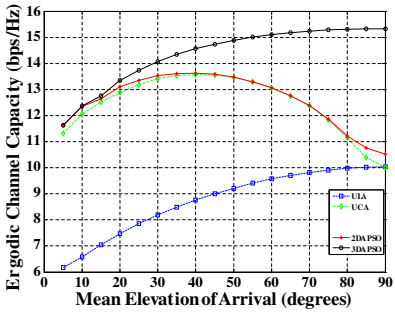

Figure 9. The ECC versus MEOA for *Example 2*.

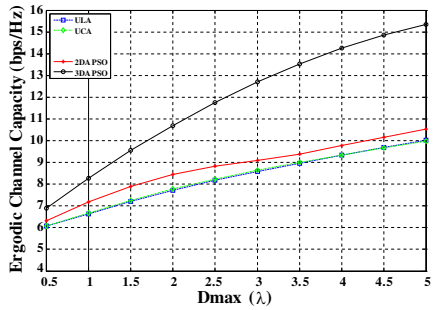

Figure 10. The ECC versus $D_{\max}$ for *Example 3*.

Table 1. The array element positions after performing the optimization process for *Example 2* with MEOA = 20°. 2DA PSO and 3DA PSO denote the cases with $\sqrt{x_{mo}^2 + y_{mo}^2} \leq D_{\max}$ and $\sqrt{x_{mo}^2 + y_{mo}^2 + z_{mo}^2} \leq D_{\max}$, respectively. E_i designates the ith array element, $i = 1, 2, \ldots, 6$.

2DA PSO	E_1	E_2	E_3	E_4	E_5	E_6
x (in λ)	4.6626	4.6626	0.0000	0.0000	−4.6626	−4.6626
y (in λ)	1.8055	−1.8055	−5.0000	5.0000	1.8055	−1.8055
z (in λ)	0.0000	0.0000	0.0000	0.0000	0.0000	0.0000

3DA PSO	E_1	E_2	E_3	E_4	E_5	E_6
x (in λ)	4.6606	4.6603	−0.0002	−0.0002	−4.6601	−4.6608
y (in λ)	1.6967	−1.6968	−4.6917	4.6921	1.6980	−1.6950
z (in λ)	−0.6322	0.6345	1.7285	−1.7275	−0.6327	0.6354

process presented in Section 3.6. Again, we observe that the proposed method provides the best ECC performance for a multiple antenna array with an optimum 3-D geometry. Moreover, the ECC with a 2-D multiple antenna array can be significantly improved by using the proposed method as compared to that with a UCA. Table 2 lists the array element positions after performing the optimization process for this example with $D_{\max} = 5\lambda$. We observe from the table that the obtained optimum 3-D array geometry is almost equal to a sphere with radius equal to $D_{\max} = 5\lambda$. However, we note that the resulting optimum 2-D array geometry is not the same as a 2-D UCA with radius equal to $D_{\max} = 5\lambda$. This confirms the results shown by Figure 10 for the 2-D case.

Table 2. The array element positions after performing the optimization process for *Example 3* with $D_{\max} = 5\lambda$. 2DA PSO and 3DA PSO denote the cases with $\sqrt{x_{mo}^2 + y_{mo}^2} \leq D_{\max}$ and $\sqrt{x_{mo}^2 + y_{mo}^2 + z_{mo}^2} \leq D_{\max}$, respectively. E_i designates the ith array element, $i = 1, 2, \ldots, 6$.

2DA PSO	E_1	E_2	E_3	E_4	E_5	E_6
x (in λ)	4.9853	3.2425	2.6160	−3.0146	−3.2536	−4.9979
y (in λ)	0.3831	3.0024	−4.1782	3.7000	−2.4743	0.1418
z (in λ)	0.0000	0.0000	0.0000	0.0000	0.0000	0.0000

3DA PSO	E_1	E_2	E_3	E_4	E_5	E_6
x (in λ)	4.9983	3. 0331	2.7312	−2.7019	−3.0249	−4.9980
y (in λ)	0.0012	0.0036	0.0045	−0.0073	0.0028	0.0104
z (in λ)	−0.1297	3.9749	−4.1882	4.2071	−3.9812	0.1399

5. CONCLUSION

This paper has presented the analytical formula for computing the spatial correlation of three-dimensional (3-D) antenna array systems under a uniform angular distribution. Using the theoretical formulas, one can compute the spatial correlation for any two different array elements located in the 3-D coordinate system. It has been observed from the simulation results that the spatial correlation decreases more rapidly as the distance between array elements increases for larger angular spread. Moreover, some spatial correlation may decrease like a sinc vibration as the angular spread increases if the distance between array elements is large enough. Based on the spatial correlation formula, we have further presented a method based on a particle swarm optimization algorithm with a proposed objective function to deploy a multiple antenna array in a wireless communication system for maximizing the ergodic channel capacity. The simulation results have confirmed the validity of the closed-form formulas and the effectiveness of the proposed method.

ACKNOWLEDGMENT

This work was supported by the National Science Council of TAIWAN under Grants NSC97-2221-E002-174-MY3 and NSC100-2221-E002-200-MY3.

REFERENCES

1. Naguib, A. F., "Adaptive antenna for CDMA wireless network," Ph.D. Thesis, Standford University, Palo Alto, CA, Aug. 1996.
2. Fulghun, T. and K. Molnar, "The Jakes fading model incorporating angular spread for a disk of scatters," *Proc. IEEE Veh. Technol. Conference (VTC'98)*, 489–493, May 1998.
3. Oestges, C. and B. Clerckx, *MIMO Wireless Communications*, Academic Press, Orlando, FL, 2007.
4. Shiu, D., G. J. Foschini, M. J. Gans, and J. M. Kahn, "Fading correlation and its effect on the capacity of multielement antenna systems," *IEEE Trans. on Communications*, Vol. 48, No. 3, 502–513, Mar. 2000.
5. Fang, L., G. Bi, and A. C. Kot, "New method of performance analysis for diversity reception with correlated Rayleigh-fading signals," *IEEE Trans. on Vehicular Technology*, Vol. 49, No. 5, 1807–1812, Sep. 2000.
6. Abdi, A. and M. Kaveh, "A space-time correlation model for multielement antenna systems in mobile fading channels," *IEEE J. on Selected Areas in Communications*, Vol. 20, No. 3, 550–560, Apr. 2002.
7. Tsai, J.-A., M. Buehrer, and B. D. Woerner, "BER performance of a uniform circular array versus a uniform linear array in a mobile radio environment," *IEEE Trans. on Wireless Communications*, Vol. 3, No. 3, 695–700, May 2004.
8. Cao, W. and W. Wang, "Effects of angular spread on smart antenna system with uniformly linear antenna array," *Proc. of IEEE 10th Asia-Pacific Conference on Communications and 5th International Symposium on Multi-dimensional Mobil Communications*, 174–178, Beijing, China, Aug. 2004.
9. Park, C.-K. and K.-S. Min, "A study on spatial correlation characteristic of array antenna for multi antenna system," *Proc. of IEEE Asia-Pacific Microwave Conference*, Vol. 3, Dec. 4–7, 2005.
10. Schumacher, L., K. I. Pedersen, and P. E. Mogensen, "From antenna spacings to theoretical capacities — Guidelines for simulating MIMO systems," *Proc. IEEE 13th International Symposium on Personal, Indoor and Mobile Radio Communications*, Vol. 2, 587–592, Lisboa, Portugal, Sep. 2002.
11. Zhou, J., S. Sasaki, S. Muramatsu, H. Kikichi, and Y. Onozato, "Spatial correlation for a circular antenna array and its applications in wireless communications," *Proc. of IEEE Global Telecommunications Conference*, Vol. 2, 1108–1113, San

Francisco, CA, USA, Dec. 2003.

12. Tsai, J.-A., M. Buehrer, and B. D. Woerner, "Spatial fading correlation function of circular antenna arrays with Laplacian energy distribution," *IEEE Communications Letters*, Vol. 6, 178–180, May 2002.
13. Tsai, J.-A. and B. D. Woerner, "The fading correlation function of a circular antenna array in mobile radio environment," *Proc. of IEEE Global Telecommunications Conference*, Vol. 5, 3232–3236, San Antonio, TX, USA, Nov. 2001.
14. Chan, S. C., H. H. Chen, and K. L. Ho, "Adaptive beamforming using uniform concentric circular arrays with frequency invariant characteristics," *Proc. of IEEE International Symposium on Circuits and Systems*, 4321–4324, May 2005.
15. Chan, S. C. and H. H. Chen "Uniform concentric circular arrays with frequency-invariant characteristics — Theory, design, adaptive beamforming and DOA estimation," *IEEE Trans. on Signal Processing*, Vol. 55, No. 1, 165–177, Jan. 2007.
16. Chen, H. H., S. C. Chan, and K. L. Ho, "Adaptive beamforming using frequency invariant uniform concentric circular arrays," *IEEE Trans. on Circuits and Systems — I*, Vol. 54, No. 7, 1938–1949, Sep. 2007.
17. Lee, J.-H. and S.-I. Li, "Spatial correlation characteristics of antenna systems using uniform concentric ring arrays," *Proc. of The 16th International Conference on Digital Signal Processing*, Santorini, Greece, Jul. 2009.
18. Eggers, P. C. F., I. Z. Kovác, and K. Olesen, "Penetration effects on XPD with GSM 1800 handset antennas, relevant for BS polarization diversity for indoor coverage," *Proc. IEEE Vehicular Technology Conference*, Vol. 13, 1959–1963, Ottawa, Canada, May 1998.
19. Kuchar, A., J. P. Rossi, and E. Bonek, "Directional macro-cell channel characterization from urban measurements," *IEEE Trans. on Antennas and Propag.*, Vol. 48, No. 2, 137–146, Feb. 2000.
20. Fulh, J., J. P. Rossi, and E. Bonek, "High-resolution 3-D direction-of-arrival determination for urban mobile radio," *IEEE Trans. on Antennas and Propag.*, Vol. 45, No. 4, 672–682, Apr. 1997.
21. Yong, S. K. and J. S. Thompson, "A three-dimensional spatial fading correlation model for uniform rectangular arrays," *IEEE Antennas and Wireless Propagation Letters*, Vol. 2, 182–185, 2003.
22. Yong, S. K. and J. S. Thompson, "Three-dimensional spatial fading correlation models for compact MIMO receivers," *IEEE*

Trans. on Wireless Communications, Vol. 4, No. 6, 2856–2869, Nov. 2005.

23. Saeed, M. A., B. M. Ali, S. Khatun, M. Ismail, and A. Rostami "Spatial and temporal fading correlation of uniform linear antenna array in three-dimensional signal scattering," *Proc. of Asia-Pacific Conference on Communications*, 425–429, Perth, Australia, Oct. 2005.
24. Raj, J. S. K., A. S. Prabu, N. Vikram, and J. Schoebel, "Spatial correlation and mimo capacity of uniform rectangular dipole arrays," *IEEE Antennas and Wireless Propagation Letters*, Vol. 7, 97–100, 2008.
25. Chuah, C.-N., J. M. Kahn, and D. N. C. Tse, "Capacity scaling in MIMO wireless systems under correlated fading," *IEEE Trans. Information Theory*, Vol. 48, No. 3, 637–650, Mar. 2002.
26. Shiu, D.-S., G. J. Foschini, M. Gans, and J. M. Kahn, "Fading correlation and its effect on the capacity of multielement antenna systems," *IEEE Trans. on Communications*, Vol. 48, No. 3, 502–513, Mar. 2000.
27. Goldsmith, A., S. A. Jafar, N. Jindal, and S. Vishwanath, "Capacity limits of MIMO channel," *IEEE Journal on Selected Area in Communications*, Vol. 21, No. 5, 684–702, Jun. 2003.
28. Kennedy, J. and R. Eberhart, "Particle swarm optimization," *Proc. of IEEE International Conference on Neural Networks*, Vol. 4, 1942–1948, 1995.
29. Kawakami, K. and Z. Meng, "Improvement of particle swarm optimization," *PIERS Online*, Vol. 5, No. 3, 261–264, 2009.
30. Kang, M. and M. S. Alouini, "Capacity of correlated MIMO Rayleigh channels," *IEEE Trans. on Wireless Communications*, Vol. 5, No. 1, 143–155, Jan. 2006.
31. Kiessling, M., J. Speidel, I. Viering, and M. Reinhardt, "A closed-form bound on correlated MIMO channel capacity," *Proc. of IEEE 56th Fall Vehicular Technology Conference*, Vol. 2, 859–863, 2002.
32. Khodier, M. M. and C. G. Christodoulou, "Linear array geometry synthesis with minimum sidelobe level and null control using particle swarm optimization," *IEEE Trans. on Antennas and Propag.*, Vol.53, No. 8, 2674–2679, Aug. 2006.
33. Shin, H., M. Z. Win, J. H. Lee, and M. Chiani, "On the capacity of doubly correlated MIMO channels," *IEEE Trans. on Wireless Communications*, Vol. 5, No. 8, 2253–2265, Aug. 2006.
34. Mangoud, M. A.-A., "Optimization of channel capacity for indoor MIMO systems using genetic algorithm," *Progress In*

Electromagnetic Research C, Vol. 7, 137–150, 2009.

35. Van Trees, H. L., *Optimum Array Processing, Part IV of Detection, Estimation, and Modulation Theory*, Wiley-Interscience, John-Wiley and Sons, New York, 2002.
36. Andersen, J. B. and K. I. Pedersen, "Angle-of-arrival statistics for low resolution antenna," *IEEE Trans. on Antennas and Propag.*, Vol. 50, No. 3, 391–395, Mar. 2002.
37. Lee, J.-H. and S.-I. Li, "Three-dimensional spatial correlation characteristics of concentric ring antenna array systems," *Proc. of the 17th International Conference on Digital Signal Processing*, T2B.4, 2011.